Accepted for publication in *Journal of Physics: Condensed Matter* (2018)

Sawtooth structure formation under nonlinear-regime ion bombardment

Joy C. Perkinson[1†], Jennifer M. Swenson[2], Alexander DeMasi[3], Christa Wagenbach[4], Karl F. Ludwig, Jr.[4], Scott A. Norris[2], Michael J. Aziz[5††]

1. The Charles Stark Draper Laboratory, Inc., Cambridge, MA 02139; 2. Southern Methodist University Department of Mathematics, Dallas, TX 75275; 3. Signature Science, Austin, TX 78759; 4. Boston University Department of Physics, Boston, MA 02215; 5. Harvard University School of Engineering and Applied Sciences, Cambridge, MA 02138

E-mail: † joyperkinson@gmail.com, †† maziz@harvard.edu

April 16, 2018

Abstract. Linear-regime Ar^+ bombardment of Si produces symmetrical ripple structures at ion incidence angles above 45° measured off-normal [1]. In the nonlinear regime, new behaviors emerge. In this paper, we present experimental results of ion bombardment that continues into the nonlinear regime until pattern saturation at multiple ion incidence angles, showing the evolution of their grazing incidence small-angle x-ray scattering (GISAXS) spectra as well as atomic force microscopy (AFM) topographs of the final, saturated structures. Asymmetric structures emerge parallel to the direction of the projected ion beam on the sample surface, constituting a height asymmetry not found in the linear regime. We then present simulations of surface height evolution under ion bombardment using a nonlinear partial differential equation developed by Pearson and Bradley [2]. We present simulated GISAXS spectra from these simulations, as well as simulated scattering from a sawtooth structure using the FitGISAXS software package [3], and compare the simulated spectra to those observed experimentally. We find that the model based on the equation by Pearson and Bradley reproduces the sawtooth structures and reproduces the nearly-flat final GISAXS spectra observed experimentally perpendicular to the sawtooth structures. However, the model fails to reproduce the final GISAXS spectra observed parallel to the sawtooth structures.

Keywords: ion bombardment, silicon, argon, nonlinear evolution equation, GISAXS, nanopatterning, sawtooth structure

1. Introduction

Nanoscale topographic pattern self-organization under low energy ($\sim$ 0.1–30 keV) ion bombardment has been an active field of study for half a century [4–15]. Much of

the work has focused on the so-called "linear regime" of pattern formation, at early times and low fluence, in which the amplitude variations of the target surface are still small. These structures can be formed using low-flux ion sources, and the mathematics describing their evolution is relatively simple: because the linear regime incorporates only small surface amplitudes, nonlinear terms in the governing equations, containing powers of the amplitude or slope, are assumed to be negligible. This general approach has been used widely because it pairs an accessible experimental regime to a convenient mathematical approach.

Despite this focus on the linear regime, recent grazing incidence small-angle x-ray scattering (GISAXS) experiments [16] have suggested that the underlying assumptions break down at lower fluences than previously expected [10, 17, 18]. Furthermore, nonlinear-regime behavior could specifically be of interest to applications requiring higher-amplitude surface structures, such as micromechanics, microprocessor integration, data storage, and photonic band gap waveguides. One nonlinear-regime morphology in particular, the sawtooth structure, was proposed as a thin film growth template by Adams *et al.* in their paper that reported sawtooth formation on diamond under 20 keV Ga^+ bombardment [19]. Other experimental studies have demonstrated that sawtooth structures form at sufficiently large fluence under Ar^+ bombardment of Si at energies as low as 1.2 keV [20] and as high as 120 keV [21], suggesting that sawtooth structures are relatively easy to grow.

Models have recently been developed to include nonlinear terms, which in principle allows them to describe behavior at larger fluences, when surface slopes are higher. The lowest-order, quadratic nonlinear terms were added by Cuerno and Barabási, resulting in the anisotropic Kuramoto-Sivashinsky (aKS) equation [22]. However, while simulations with the aKS equation result in disordered ripple structures, they fail to reproduce the anisotropic sawtooth structures observed experimentally in the nonlinear regime [19–21].

Two essential features of evolving sawtooth structures are (a) the presence of alternating faces with very different slopes, and (b) the uniform, shock-like motion of these sloped faces. A successful model must therefore accurately describe the sputter yield over a wide range of local incidence angles, and give rise to shock-like behavior. A model with these features was first demonstrated by Chen [23] and Holmes-Cerfon [24, 25] who studied the evolution of nearly-vertical walls under normal incidence ion irradiation, using a model that included the full angle-dependent sputter yield $Y(u_x)$, where $u(x)$ is the amplitude of the bombarded surface and x is the direction parallel to the projected incoming ion beam. This model demonstrates how two faces with very different slopes are connected using corner solutions and evolve under ion bombardment using the mathematics characteristic of a propagating shock front. More recently, in a study of terrace formation under nearly-grazing incidence ion bombardment of initially flat surfaces, Pearson and Bradley introduced a model in which $Y(u_x)$ was expanded to third order in u_x [2]. Though in principle limited to relatively small slopes, this approach qualitatively captures the relevant behavior of terraced sawtooth surfaces, and is also

easier to discretize for numerical simulation, and for these reasons, we adopt it here.

In this paper, we investigate nonlinear-regime pattern formation through both experiment and simulation. Experimentally, we investigate the topographic pattern formation on Si(001) targets under 1 keV Ar^+ ion bombardment at the full range of angles corresponding to surface roughening parallel to and perpendicular to the projected ion beam. We examine atomic force microscopy (AFM) topographs of late-stage, "saturated" patterns after roughening has reached steady state at all roughening angles, and we present two AFM topographs of early-stage nonlinear roughening. We then present GISAXS scattering spectra from targets bombarded in the nonlinear regime at long times and fluences above 10^{19} ions/cm^2.

We compare these experimental results to simulations based on the the aKS equation with an added cubic nonlinear term, as presented by Pearson and Bradley [2]. The equation presented in that paper is one-dimensional; when the equation is written for a two-dimensional surface, it takes the form

$$u_t = \beta_1 u_{xx} + \beta_2 u_{yy} + \gamma_1 u_{xxxx} + 2\gamma_2 u_{xxyy} + \gamma_3 u_{yyyy} + \delta_1 u_x^2 + \delta_2 u_y^2 + \frac{1}{6}\epsilon_1 u_x^3 + \frac{1}{6}\epsilon_2 u_y^3, \quad (1)$$

where $u(x, y, t)$ is the amplitude of the bombarded surface, x and y refer to the directions parallel and perpendicular to the projected incoming ion beam, respectively, and the parameters β, γ, δ, and ϵ are the coefficients of the terms in the partial differential equation. The parameter ϵ is defined for the x direction in the publication by Pearson and Bradley [2], and is related to the atomic volume, ion flux, and angle-dependent sputter yield of the physical system. We present simulations of surface evolution based on Equation 1 and compare them to experimentally-observed roughening in the nonlinear regime.

We also present simulations of GISAXS spectra, both from the simulated structures resulting from evolution under Equation 1 as well as from idealized sawtooth structures. One difficulty surrounding nonlinear-regime data is that analysis of GISAXS scattering spectra is no longer straightforward. When the product of the structure amplitude a and the wavenumber q is $aq \ll 1$, then the GISAXS intensity is proportional to the structure factor of the sample surface [26]. This approximation is generally valid in the linear regime. However, in the nonlinear regime, structure amplitudes grow large enough that this condition is no longer satisfied, and so the GISAXS scattering intensity profiles are no longer proportional to the structure factor of the surface. It is therefore significantly more difficult to infer information about the surface structures producing the recorded GISAXS profiles in the nonlinear regime. Interpretation of experimental nonlinear-regime GISAXS data can be aided by the presentation of simulated GISAXS spectra. Thus, one of our aims is to compute the GISAXS structure factor of simulated sawtooth structures for direct comparison to experimental results. In this paper, we discuss how the two methods we use to simulate GISAXS spectra can reproduce the experimentally-observed characteristics of sawtooth evolution.

2. Methods

2.1. Experimental

Samples are polished p-doped Si (001) with resistivity 1–10 Ω·cm from Virginia Semiconductor Inc. For the two early-time samples presented as part of a nonlinear roughening time series, sample preparation, geometry, vacuum chamber, and procedures are identical to those described by Madi *et al.* in reference [1], with the only difference being that the base vacuum pressure of the vacuum chamber is 2×10^{-8} Torr.

All other samples, analyzed via GISAXS until pattern saturation, are bombarded *in situ* during simultaneous GISAXS data collection. For these samples, sample size is 3.2×3.2 cm^2 in order to cover the raised portion of the Mo sample platen, minimizing the effects of metallic impurity incorporation into the sample via redeposition of sputtered material from the platen. Samples are affixed to the sample platen using molten In shielded from the path of the beam by the sample itself. Care is taken to mount the sample in the chamber in a geometry that minimizes the incorporation of metallic impurities due to secondary collisions, and chamber walls and fixtures near the sample are covered with large silicon wafers to further reduce line of sight of the beam to metallic components that could result in sputtering and redeposition of metal onto the sample. The ion source is a Veeco DC source with 3 cm graphite grids in a flange mount configuration, with an ion energy of 1 keV and a flux of 3×10^{15} ions/cm^{2}s reckoned in a plane normal to the ion beam direction. Bombardment is performed using high-purity Ar^+ at a working pressure of 1×10^{-4} Torr over a base pressure of approximately 1×10^{-8} Torr. Bombardment angles were 50°–85° off-normal, corresponding to the range of angles that produce roughening for this combination of target material, ion species, and ion energy. GISAXS data were taken both parallel and perpendicular to the direction of the projected ion beam for each bombardment angle considered.

GISAXS is performed at beamline X21 of the National Synchrotron Light Source (NSLS) at Brookhaven National Laboratory, using a custom vacuum chamber in a dedicated facility for the study of surface and thin-film processes. The x-ray photon flux is approximately 10^{12} photons/s, with a wavelength 0.124 nm selected by a Si(111) monochromator. Photon incidence angle onto the sample is 0.82°, and scattered photons are captured by a 487×195-pixel PILATUS detector [27].

When collecting GISAXS data, samples are first bombarded *in situ* under vacuum to remove the native oxide layer and to amorphize and smoothen the surface layer. All samples are bombarded at incidence angles corresponding to pattern amplification, because bombardment of high-amplitude structures at those incidence angles leads to steep feature formation rather than smoothening [28]. Data are collected at selected ion fluences throughout bombardment by the PILATUS area detector. To ensure high photon fluence without overloading the detector, data are collected for multiple intervals at each selected ion fluence and then averaged together. Sample bombardment continues until surface pattern saturation, at which point no visible changes to the GISAXS profile

are produced by further bombardment by at least 5×10^{18} ions/cm^2.

The final surface structures produced during experiments are imaged using AFM at Harvard University's Center for Nanoscale Systems. AFM topographs are analyzed using WSxM software [29], which also calculates the fast Fourier transform (FFT) of the sample surface.

2.2. Numerical

Simulations of Equation 1 are performed using a standard finite difference scheme using centered differences for spatial derivatives. Because one of our aims is to compute the simulated GISAXS structure factor given by Equation 2.4 in Sinha *et al.* [26], a large domain is preferable to reduce noise in the ultimate result. Then, because the domain is large, each timestep is expensive, so that an unconditionally stable timestepping method such as Crank-Nicholson is preferrable to allow relatively large timesteps. However, because the governing equation is nonlinear, each Crank-Nicholson step therefore requires the solution of a large nonlinear algebraic system, and the central difficulty in such an approach is to solve such systems quickly.

For this purpose, we adopt the Portable, Extensible Toolkit for Scientific Computation (PETSc), a C library providing highly-parallelized iterative solvers for both linear and nonlinear systems of equations [30–32]. This capability makes it an ideal platform for the solution of discretized PDEs on large domains, and it provides specific functionality to this end. The resulting code is run on Southern Methodist University's ManeFrame cluster using up to 1024 nodes. Post-processing to obtain simulated AFM images and GISAXS spectra is then performed using Python and Matplotlib. The simulated AFM images are made by applying a grayscale color mapping to the surface amplitudes $u(x, y)$ for a given simulation time t. To create GISAXS spectra, simulated two-dimensional patterns in q_x and q_y are calculated from the structure factor equation given by Sinha *et al.* in their Equation 2.4 [26], and values along the axes $q_x = 0$ and $q_y = 0$ are recorded.

In addition to the above approaches, we have calculated simulated 2-dimensional (2D) GISAXS scattering spectra for a simple sawtooth ripple structure using the software package FitGISAXS [3]. FitGISAXS allows the construction of virtual surfaces using stacked layers of material, allowing the placement of sawtooth ripples atop a Si substrate. The scattering is then calculated using the distorted-wave Born approximation used to describe the scattering of grazing-incidence small-angle x-rays, including reflection and refraction, from a simulated surface [26, 33]. The simulated sawtooth surface is a 1D paracrystal consisting of teeth spaced 36 nm apart, with a standard deviation of 10 nm. Each sawtooth ripple is 12 nm wide, 100 nm long, and 1.56 nm tall. The asymmetry of the sawtooth is chosen to be the largest possible value, to encourage replication of the asymmetrical GISAXS pattern observed in some experiments. The material of the ripples and the underlying substrate is chosen to be Si, which is specified using the complex form of the refractive index for Si. The real

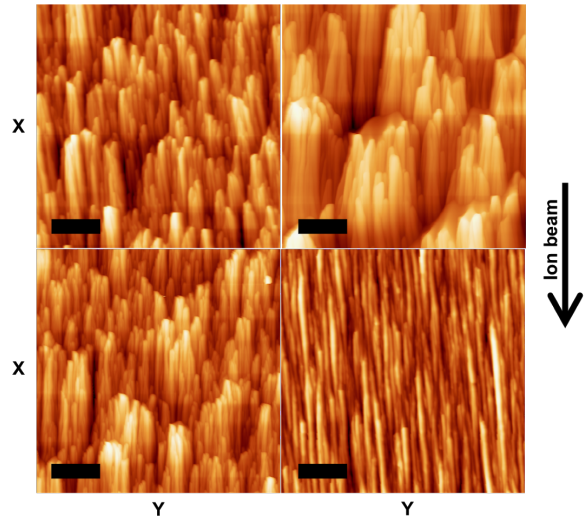

Figure 1. AFM topographs of sample morphology saturation under 55° (top left), 70° (top right), 75° (bottom left), and 85° (bottom right) bombardment of Si by Ar^+ ions. Height scales, bombardment times, and fluences are 354 nm, 300 minutes, 5.4×10^{19} ions/cm^2; 320 nm, 120 minutes, 2.2×10^{19} ions/cm^2; 389 nm, 91 minutes, 1.6×10^{19} ions/cm^2; and 132 nm, 305 minutes, 5.5×10^{19} ions/cm^2, respectively. Scale bars, shown as horizontal black lines, are 400 nm for the 75° sample and 1 μm for the other three samples. The projected ion beam direction is from the top to the bottom of the page.

component, $\delta = 3.8 \times 10^{-6}$, of the refractive index, and the imaginary component, $\beta = 4.5 \times 10^{-8}$ are retrieved from Lawrence Berkeley National Laboratory's online lookup tables [34] based on published atomic and nuclear data tables [35].

3. Experimental sawtooth formation

In this section, we present AFM topographs of samples bombarded to pattern saturation in the nonlinear regime along with their associated GISAXS spectra, both of which reveal sawtooth formation.

3.1. Direct observation of sawtooth formation and structure saturation

Pattern saturation is achieved at sufficiently high fluences for ion incidence angles between 55° and 85°. Under AFM, amplitudes are measured to be between 100 and 400 nm for these saturated structures, compared with a typical 1–10 nm for linear-regime rippled samples [1]. The surface structures exhibit characteristic lateral wavelengths in the hundreds of nm, which interfere structurally with visible light and create a cloudy appearance to sample surfaces at many bombardment incidence angles.

Examples of the saturated patterns resulting from bombardment angles 55°, 70°, 75°, and 85° are shown in Figure 1. For each sample shown, the projected ion beam direction is from the top to the bottom of the page. Sawtooth structures are visible in

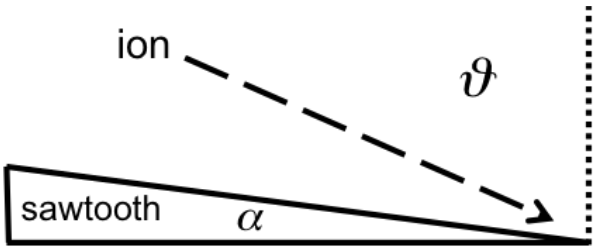

Figure 2. The emergence of sawtooth structures decreases the local incidence angle between the surface and the incoming ion beam. If the initial ion incidence angle is θ, and a sawtooth forms during ion bombardment with an angle α from the horizontal, then the local ion incidence angle is $\theta + \alpha$. This increased effective incidence angle could cause the emergence of perpendicular-mode ripples at lower bombardment angles than previously observed.

all topographs, though the asymmetry is more obvious to the unaided eye at incidence angles $< 85°$. At incidence angles $< 85°$, the beam-facing edge of the sawtooth forms a chevron-like shape, particularly visible at 70°. In all cases the short side of the sawtooth structure is facing the direction of the ion beam, and is an x-direction asymmetry ("parallel-mode," with wave vector parallel to the projected ion beam direction). The x direction is on the vertical axis in the topographs, which departs from mathematical tradition but conforms with common practice in the field of experimental ion bombardment. In the y-direction (the horizontal axis in Figure 1, "perpendicular-mode", with wave vector perpendicular to the projected ion beam direction), structures are visible on many length scales. The variation of length scales is particularly evident for the 70° sample, in which structures range from approximately $30 - 500$ nm.

Unlike samples in the linear regime of pattern roughening, ripple orientation is difficult to determine by visual examination of AFM topographs. FFT analysis of the AFM topographs is therefore used to ascertain the orientation of the dominant patterns for each sample. At angles $\geq 80°$, perpendicular-mode roughening dominates pattern formation, similar to observed behavior in the linear regime. Samples bombarded in the angle range $55° - 75°$ exhibit significant contributions from both parallel-mode and perpendicular-mode roughening.

The emergence of perpendicular-mode structures at incidence angles $55° - 75°$ is in contrast with linear-regime roughening studies [1, 10, 17]. In the linear regime, these incidence angles correspond only with parallel-mode roughening, while perpendicular-mode ripples emerge at angles $> 75°$, and hole patterns that we interpret to be simultaneous roughening in both directions emerge at 75° [1]. This result could be explained by the change in effective incidence angle due to sawtooth structures with long, sloping backs such as those seen in the first three panels of Figure 1. The geometry of this change in local incidence angle is described in Figure 2. The sawtooth structures formed on the samples bombarded at $55° - 75°$ exhibit sloped faces at angles ranging from approximately $5° - 25°$ off horizontal, as revealed by the topographs in Figure

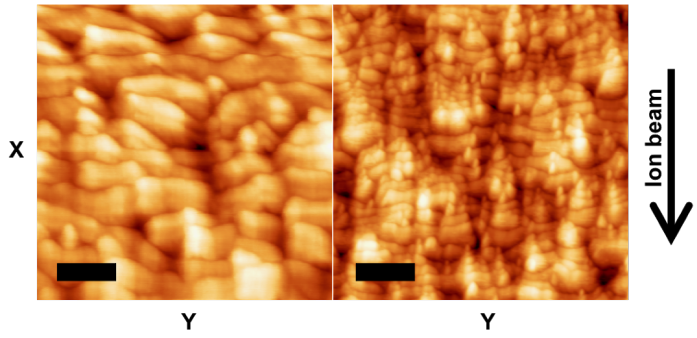

Figure 3. Early-time nonlinear structures of Si bombarded by Ar^+ at 70° for (left) 3 minutes, and (right) 16 minutes. Height scales are (left) 15 nm and (right) 21 nm. Scale bars, shown as horizontal black lines, are 100 nm (left) and 400 nm (right). The projected ion beam direction is from the top to the bottom of the page. At 3 minutes of bombardment, sawtooth structures have begun to form, with the short side of the sawtooth facing the incident ion beam. By 16 minutes of bombardment, y-direction patterns have begun to evolve.

1. The highest slopes present on observed sawtooths would be enough to bring local incidences angles into the perpendicular-mode regime even on the sample bombarded at 55°.

To observe early structures that these samples exhibit on the way to saturation, a time series is created for the specific case of the angle $\theta = 70°$. Samples are bombarded for 3 minutes and 16 minutes (5.4×10^{17} ions/cm^2 and 2.9×10^{18} ions/cm^2, respectively), and the final states are imaged using AFM. The resulting topographs are shown in Figure 3, with projected ion beam direction from the top to the bottom of the page. At 3 minutes, sawtooth structures have begun to form, with the short side of the sawtooth facing the incident ion beam, as observed in saturated structures. At this time, the leading edges of the nascent sawtooth structures are concave downward, similar to the late-time chevron structures seen in Figure 1. Early-stage y-direction patterning is also visible. By 16 minutes, y-direction structures are clearly visible. These y-direction structures are present on all samples on which pattern saturation is observed, as seen in Figure 1. These results show that sawtooth structures are clearly present along with early-stage y-direction roughening at angles below the linear-regime y-direction roughening transition of 75° by a fluence of 5.4×10^{17} ions/cm^2, and that y-direction patterning is clearly visible by a fluence of 2.9×10^{18} ions/cm^2.

3.2. Experimental GISAXS measurements of patterns undergoing saturation

The GISAXS measurements discussed in this section are from samples bombarded using a higher-flux source than previously-reported results for 1 keV Ar^+-bombarded Si [10]. Previous linear-regime data were acquired using a source with flux 1.2×10^{12} ions/cm^{2}s, while these new results are from an ion source with flux 3×10^{15} ions/cm^{2}s. Despite this difference, we find that GISAXS measurements of surfaces patterned under high-flux

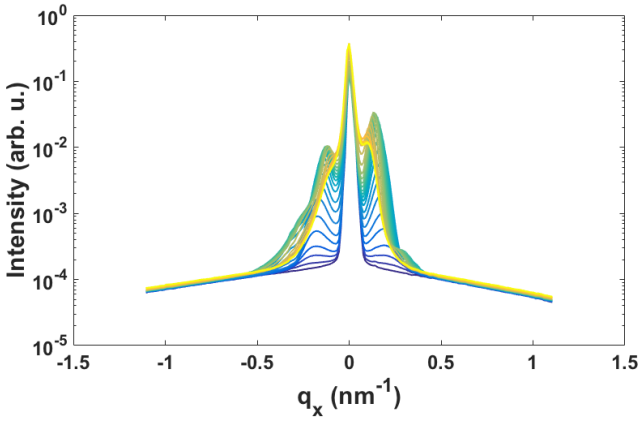

Figure 4. A typical GISAXS intensity profile in the x direction during pattern amplification to saturation at 70° incidence, showing asymmetrical scattering. The initial intensity profile, corresponding to a sample smoothened *in situ* at normal incidence, is shown in dark blue (dark gray, in black and white). Intensity profiles are shown for increasing fluences up to a saturation value of 2.43×10^{19} ions/cm^2, shown in yellow (light gray, in black and white).

ion bombardment initially exhibit intensity profiles similar to those from previously-published linear-regime data [10, 17, 18]. This observation shows that although some behavior during ion bombardment, such as stress accumulation, appear to be flux-dependent [36], the growth of unstable modes in the linear regime does not appear to be flux-dependent. The intensity profiles that we compare to earlier results correspond to the brief period the samples spend in the linear regime, when patterns are symmetrical and low-amplitude. As fluences increase past approximately 10^{17} ions/cm^2, nonlinear behaviors emerge.

Strong asymmetry emerges in the x direction, with one of the satellite peaks along the Yoneda wing, the local maximum of diffuse scattering [37], growing faster than the other. This scattering behavior corresponds to the emergence of sawtooth structures, in which one of the sides of each corrugation on the sample is shorter and steeper, while the other is longer with a shallower slope. The longer, shallower side is downstream of the sawtooth, which scatters more x-ray intensity and creates a greater-amplitude peak in the GISAXS scattering profile due to its longer length. The intensity versus wavevector versus time graphs of characteristic GISAXS measurements of nonlinear-regime x-direction roughening are presented in Figure 4.

In the y direction, no sawtooth structures form. Negligible asymmetry emerges, as is expected for corrugations oriented parallel to (with wavevector perpendicular to) an ion beam impinging on an isotropic, amorphous surface; any observed asymmetry is attributed to slight experimental misalignment. After an initial period of pattern formation and ripple coarsening, ripples of many wavelengths emerge, which we interpret to be the physical change that drives the GISAXS pattern to become "smeared out" as roughening occurs at many wavevectors at once. At the point of pattern saturation, the

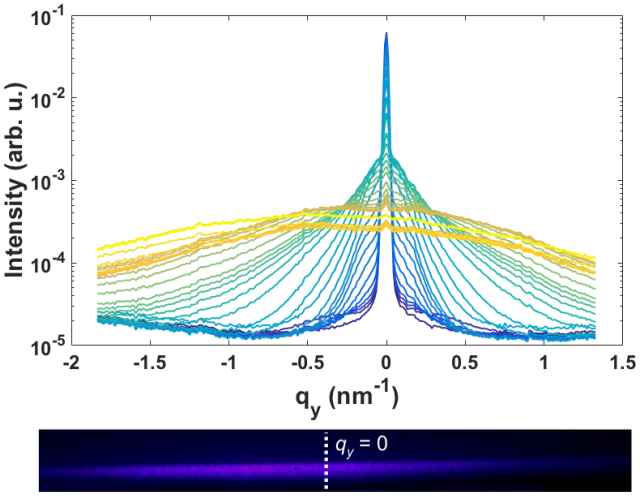

Figure 5. *(Top)* A typical GISAXS intensity profile in the y-direction during pattern amplification to saturation at 75° incidence, showing a "smeared out" final scattering profile. The initial intensity profile, corresponding to a sample smoothened at normal incidence *in situ*, is shown in dark blue (dark gray, in black and white). Intensity profiles are shown for increasing fluences up to a saturation value of 2.16×10^{19} ions/cm^2, shown in yellow (light gray, in black and white). *(Bottom)* The two-dimensional detector readout of intensity versus wavenumber, corresponding to the maximum fluence above, showing "smeared out" scattering along the Yoneda wing. The dashed line indicates the wavevector $q_y = 0$.

scattering intensity profile versus wavevector appears as a smooth curve with no single characteristic wavevector. Even the central peak at $q = 0$, which usually dominates other intensities along the Yoneda wing, barely stands out in this saturated GISAXS pattern. The intensity versus wavevector versus time graphs from typical GISAXS measurements of y-direction roughening, along with the corresponding two-dimensional detector readout for the maximum fluence, are presented in Figure 5. Because the ion incidence angle for the sample profiled in Figure 5 is 75°, at the lower end of y-direction roughening, no strong satellite peaks emerge in the GISAXS profile. Instead, intensity is amplified at all wavenumbers outside the central peak at -0.1 nm$^{-1} < q < 0.1$ nm^{-1}, while the central peak decays. The GISAXS profile of the saturated structure is a single, "smeared-out" GISAXS pattern that stretches along the length of the observed Yoneda wing.

4. Simulated sawtooth formation

In this section, we present simulations of topography evolution based on Equation 1 and their associated GISAXS spectra. We show that the asymmetrical scattering observed experimentally can also be reproduced using FitGISAXS simulations of a surface sawtooth structure.

4.1. Simulated height evolution of a two-dimensional surface

Simulations are run showing surface topography evolution under ion bombardment using Equation 1. Model coefficients are chosen in order to fulfill the conditions required for asymmetry, and are set to $\beta_1 = -1$, $\beta_2 = 0$, $\gamma_1 = -1$, $\gamma_2 = -1$, $\gamma_3 = -1$, $\delta_1 = -0.5$, $\delta_2 = -0.5$, $\epsilon_1 = 0.3$, and $\epsilon_2 = 0$. The plateaus observed on the backs of sawtooth structures at the early stages of nonlinear roughening occur only if an asymmetry in the model is introduced by setting one of the two coefficients, ϵ_1 and ϵ_2, of the cubic term to zero. The nonzero coefficient, chosen to be ϵ_1, is set to 0.3 because that value is used in the publication that presents the model [2] after consideration of physical parameters for the same experimental system used in our nonlinear roughening experiments. An 400 by 400 dimensionless grid is used with an initial condition of randomized dimensionless heights between 0 and 0.01. Early-stage patterning is shown in the top left panel of Figure 6. As height evolution continues, patterns coarsen into well-defined ripples by dimensionless simulation time $t = 500$, as shown in the top right panel of Figure 6. By $t = 1000$ (Figure 6, bottom left panel), sawtooth structures emerge. These structures coarsen into plateaus with increasing simulation time, as shown at $t = 3000$ (Figure 6, bottom right panel). This final topograph exhibits sawtooth structures as well as a large variety of length scales, both of which are observed in saturated experimental structures for incidence angles $55 - 75°$. This simulation time also shows sharp chevron-shaped structures, reminiscent of the chevron structures seen experimentally at ion incidence angles $< 85°$ in Figure 1. However, the experimental chevron structures are overlaid with perpendicular-mode ripples; because the coefficients β_1 and (in particular) β_2 are constant, Equation 1 is unable to replicate these structures. Thus, while many characteristic features of the nonlinear regime of ion bombardment are captured in this weakly-nonlinear model, it would require further refinement – with additional nonlinear terms – to more completely capture experimental behavior.

At $t = 3000$, additional evolution of 500 simulation time units produces no further qualitative change in surface features, amplitudes, or the calculated GISAXS spectra discussed below. After this point, it is assumed that nonlinear mechanisms dominate in a very slow coarsening regime. Rapid saturation followed by slow coarsening is a common behavior in nonlinear models, but it is usually difficult to assign the transition in behavior to a single term. Understanding this transition and the post-transition behavior is its own field of mathematical analysis and is outside the scope of this paper.

4.2. Simulated GISAXS at grazing incidence ion bombardment

Simulated GISAXS scattering from the surface topography evolution given by Equation 1 is given in Figure 7. At early times after surface evolution begins, scattering intensity at high wavenumbers is low, indicating an absence of structures with short real-space dimensions. As the surface evolves, the scattering approaches a near-flat spectrum. At simulation times above $t = 500$, slight asymmetry emerges, corresponding to the emergence of sawtooth structures, but otherwise little change is observed in the

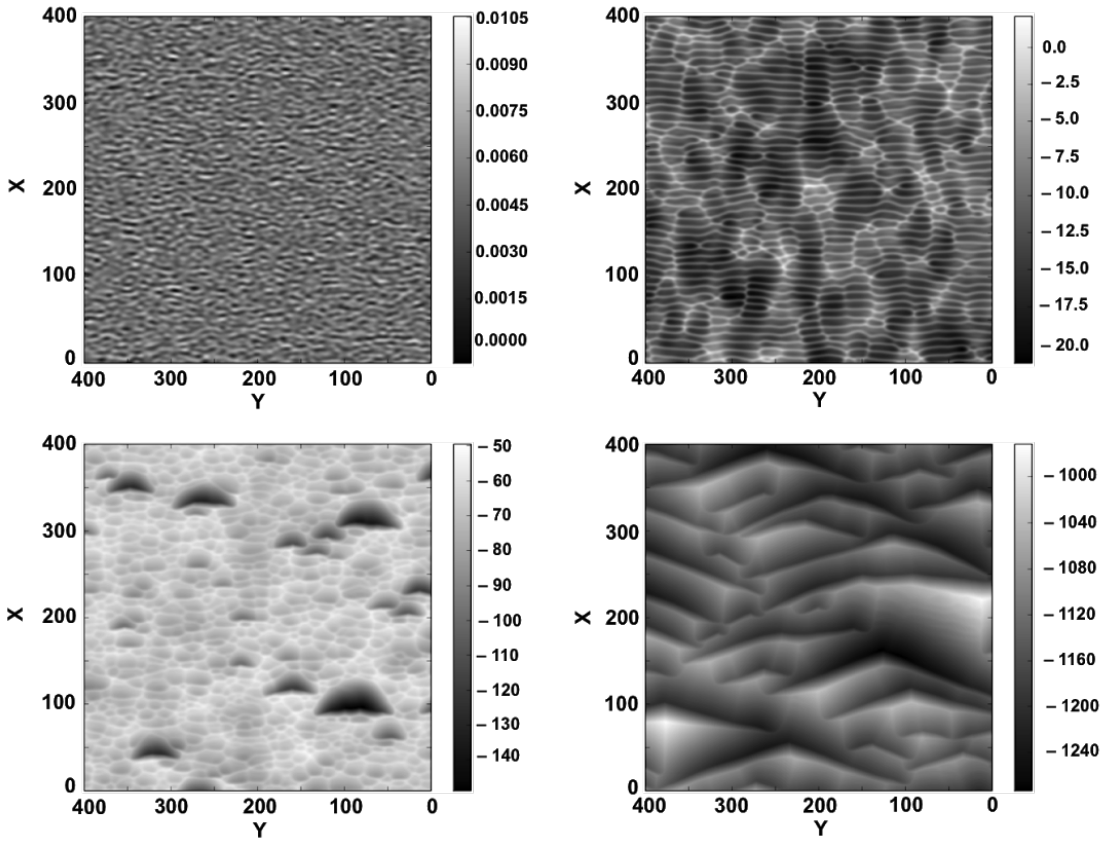

Figure 6. Maps of the sample height on a dimensionless 400 by 400 grid during height evolution according to Equation 1 with $\beta_1 = -1$, $\beta_2 = 0$, $\gamma_1 = -1$, $\gamma_2 = -1$, $\gamma_3 = -1$, $\delta_1 = -0.5$, $\delta_2 = -0.5$, $\epsilon_1 = 0.3$, and $\epsilon_2 = 0$. Dimensionless height scale bars are shown to the right of each simulated topograph. Dimensionless simulation times are (top left) 50, (top right) 500, (bottom left) 1000, and (bottom right) 3000. The initial condition is chosen by setting each pixel to a randomized height between 0 and 0.01. As evolution continues, sample heights become negative due to sputter erosion of the substrate. Patterning begins by $t = 50$ and coarsens into ripples by $t = 500$, and sawtooth structures begin to form by $t = 1000$. They coarsen into broader chevron-shaped sawtooths reminiscent of experimentally-observed structures at incidence angles $< 85°$, with a range of characteristic length scales, by $t = 3000$.

simulated GISAXS spectrum. These simulated late-time spectra are qualitatively similar to the "smeared-out" experimental results observed experimentally for y-direction roughening. However, whereas experimentally we observe these broad final scattering spectra only in the y direction, simulations based on Equation 1 yield flat late-time spectra in both x and y. We interpret these simulated flat spectra as resulting from many length scales in both directions.

Harmonic peaks emerge in the scattering spectra in Figure 7. These are a well-understood phenomenon characteristic of weakly-nonlinear equations, in which nonlinear terms containing powers of the most-unstable mode $\exp(ik^*x)$ excite modes at integer multiples of the wavenumber k^* [38, 39].

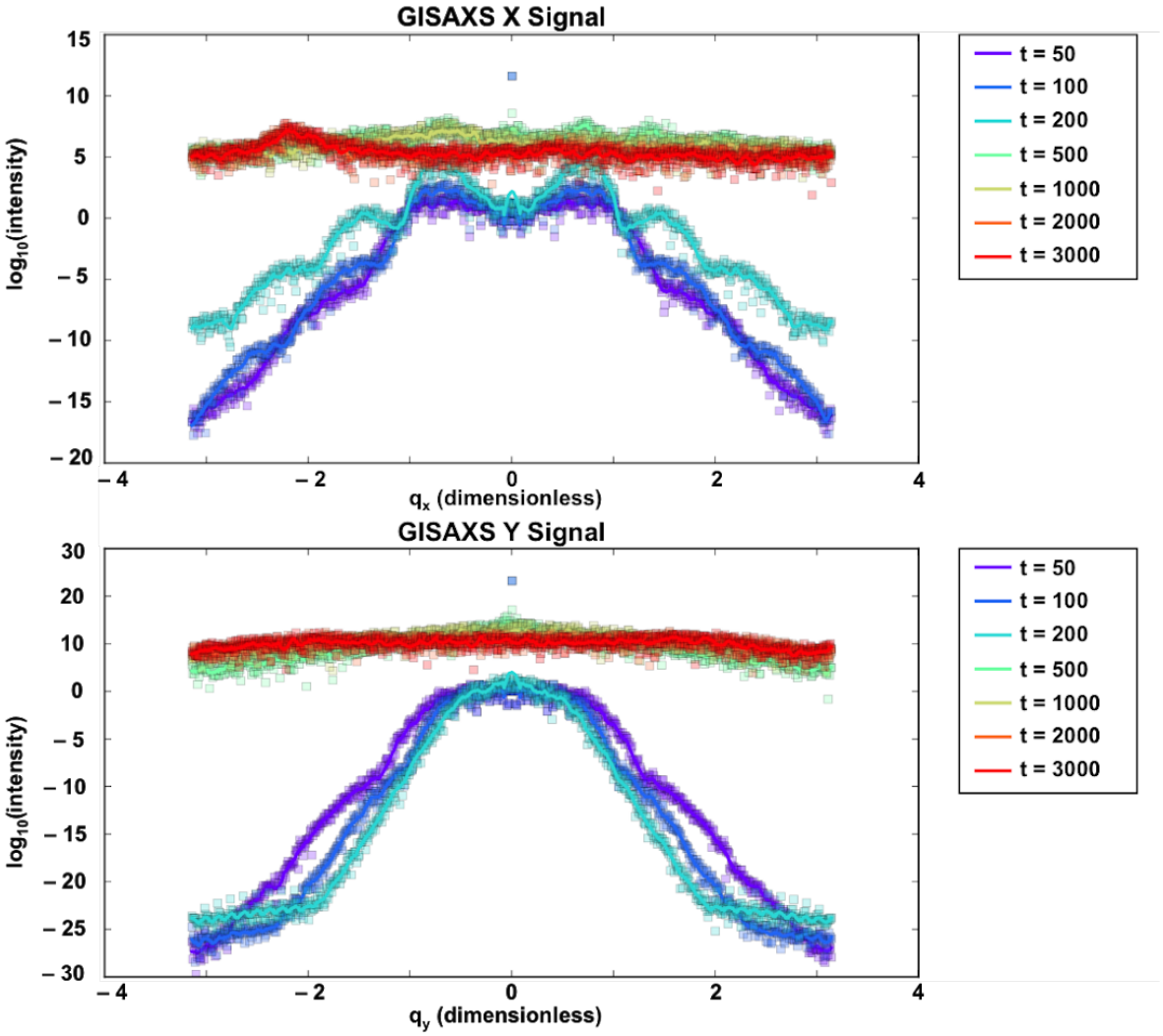

Figure 7. Scattering spectra from the simulated topography evolution of an initially-flat surface using Equation 1. Spectra are shown in both the x (top) and y (bottom) directions. Scattering from the surface during early-stage patterning is given by the purple curve, while scattering at the final simulation time, $t = 3000$, is given by the red curve. In both directions, the scattering profile is lower intensity at high wavenumber during early-stage topography evolution and evolves to the characteristic "smeared-out" scattering pattern at $t = 3000$.

Simulations of GISAXS scattering in the x direction from sawtooth structures were also performed using FitGISAXS [3]. A cross-section of the scattering, showing the intensity at the simulated two-dimensional detector, is shown in the top panel of Figure 8. The vertical line crossing the middle of the image marks the wavenumber $q_x = 0$. X-ray intensity is indicated with color, with white corresponding to highest intensity, and dark blue (dark gray in black and white prints) corresponding to lowest intensity. The bottom panel of Figure 8 shows experimental x-ray intensity reported by the two-dimensional detector during GISAXS scattering off of a Si substrate bombarded by 1

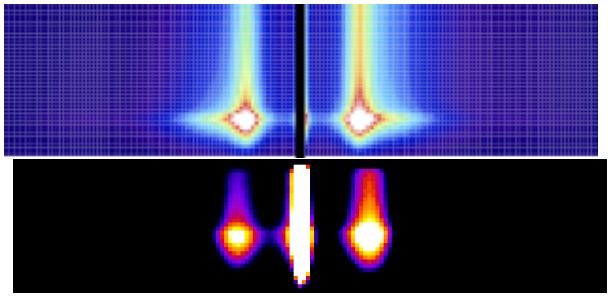

Figure 8. (Top) Simulated GISAXS intensity from a sawtooth structure using FitGISAXS simulation software. Intensity is indicated by color, from dark blue (dark gray in black and white prints, lowest intensity) to white (highest intensity). (Bottom) GISAXS data measured during 70° bombardment of Si by 1 keV Ar^+. Intensity is indicated by color, from black (lowest intensity) to white (highest intensity). Both simulated and experimental spectra exhibit asymmetrical preferential scattering to the right.

keV Ar^+ ions at 70° incidence. In the bottom panel, white indicates the highest x-ray intensity, while black indicates lowest intensity.

Simulated and experimental GISAXS spectra show asymmetrical preferential scattering to the right, due to the emergence of sawtooth structures in the nonlinear regime. Spectra from simulations based on Equation 1 show "smeared-out" final spectra in both the x and y directions (Figure 7), in agreement with experiments in the y direction, but in contrast with experiments at ion incidence angles $> 75°$ in the x direction. Spectra from x-direction FitGISAXS simulations are not "smeared-out," and are thus in better agreement with late-time experimental results from the x direction.

5. Conclusion

Nonlinear-regime roughening of Si samples under 1 keV Ar^+ bombardment has shown that with increasing fluence, samples develop sawtooth ripple structures in the x direction at angles $\leq 75°$. In the y direction, structures emerge with no single characteristic wavelength at all angles that produce roughening below the most grazing incidence (i.e. $\geq 55°$). y-direction patterning at angles $< 75°$ is attributed to the change in local incidence angle caused by large sawtooth structures.

GISAXS profiles in the x direction exhibit strong asymmetry as the result of asymmetrical sawtooth structures on the surface. GISAXS profiles in the y direction produce "smeared-out" final profiles at all incidence angles that produce roughening (i.e. $\geq 55°$).

GISAXS profiles of the nonlinear regime of sample roughening suggest that the length of the linear regime, at which scattering profiles are symmetrical about $q = 0$, is short, confined to fluences below approximately 10^{17} ions/cm^2. Structures saturate over a fluence of approximately 10^{19} ions/cm^2.

Quantitative analysis of the GISAXS data is limited by high surface structure

amplitude, which causes the scattered intensity profile to no longer be proportional to the structure factor of the surface height. However, simulations of surface roughening based on Equation 1 can reproduce many aspects of nonlinear-regime experiments, including the emergence of sawtooth structures, wavelength coarsening, and structures of many characteristic wavelengths. Simulated GISAXS scattering off of these surfaces shows the flat high-fluence scattering spectra characteristic of y-direction samples. These similarities reinforce the importance of cubic nonlinear terms in models of late-stage structural amplification under ion bombardment.

Open questions for future research include investigating why simulations based on Equation 1 produce "smeared-out" final spectra in both the x and y directions, when they are only observed experimentally in the y direction, as well as investigating applications for the high-amplitude structures presented in this paper. Interesting directions for simulations include investigating whether nonlinear roughening terms could reproduce the bidirectional roughening characteristic of the high-fluence, steady-state structures seen experimentally.

6. Acknowledgements

The work of J.C.P. and M.J.A. was supported by DE-FG-02-06ER46335 and NSF DMR-1409700. The work of J.M.S. and S.A.N. was supported by NSF DMR-1408642. The work of A.D., C.W., and K.F.L., Jr. was supported by NSF DMR-1307979. The Center for Nanoscale Systems (CNS) is a member of the National Nanotechnology Infrastructure Network, which is supported by NSF Grant ECS-0335765. CNS is part of Harvard University.

7. Author Contributions

J.C.P. performed experiments at BNL and Harvard and wrote the manuscript. J.M.S. performed simulations of Equation 1 and contributed to associated written portions of the manuscript. A.D. performed experiments at BNL. C.W. performed FitGISAXS simulations. K.F.L. supervised A.D. and C.W. and provided overall guidance. S.A.N. supervised J.M.S., contributed text to the manuscript, and provided overall guidance. M.J.A. supervised J.C.P. and provided overall guidance.

References

[1]C. S. Madi, H. B. George, and M. J. Aziz, "Linear stability and instability patterns in ion-sputtered silicon", Journal of Physics: Condensed Matter **21** (2009) `http://dx.doi.org/10.1088/0953-8984/21/22/224010`.

[2]D. A. Pearson and R. M. Bradley, "Theory of terraced topographies produced by oblique-incidence ion bombardment of solid surfaces", Journal of Physics: Condensed Matter **27**, 015010 (2015).

[3]D. Babonneau, "FitGISAXS: software package for modelling and analysis of GISAXS data using IGOR Pro", Journal of Applied Crystallography **43**, 929–936 (2010).

[4]M. Navez, C. Sella, and D. Chaperot, "Microscopie électronique – Étude de l'attaque du verre par bombardement ionique. (French) [electron microscopy – Study of the irradiation of glass by ion bombardment]", Comptes Rendus Hebdomadaires Des Séances De L'Académie des Sciences **254**, 240–242 (1962).

[5]P. Sigmund, "A mechanism of surface micro-roughening by ion bombardment", Journal of Materials Science **8**, 1545–1553 (1973).

[6]R. M. Bradley and J. M. E. Harper, "Theory of ripple topography induced by ion bombardment", Journal of Vacuum Science and Technology A **6**, 2390–2395 (1988).

[7]G. Carter and V. Vishnyakov, "Roughening and ripple instabilities on ion-bombarded Si", Physical Review B **54**, 17647–17653 (1996).

[8]C. C. Umbach, R. L. Headrick, and K.-C. Chang, "Spontaneous nanoscale corrugation of ion-eroded SiO_2: the role of ion-irradiation-enhanced viscous flow", Physical Review Letters **87** (2001) `http://dx.doi.org/10.1103/PhysRevLett.87.246104`.

[9]M. Moseler, P. Gumbsch, C. Casiraghi, A. C. Ferrari, and J. Robertson, "The ultrasmoothness of diamond-like carbon surfaces", Science **309**, 1545–1548 (2005).

[10]C. S. Madi, E. Anzenberg, K. F. Ludwig, Jr., and M. J. Aziz, "Mass redistribution causes the structural richness of ion-irradiated surfaces", Physical Review Letters **206** (2011) `http://dx.doi.org/0.1103/PhysRevLett.106.066101`.

[11]S. A. Norris, J. Samela, L. Bukonte, M. Backman, F. Djurabekova, K. Nordlund, C. S. Madi, M. P. Brenner, and M. J. Aziz, "Molecular dynamics of single-particle impacts predicts phase diagrams for large scale pattern formation", Nature Communications **2** (2011) `http://dx.doi.org/10.1038/ncomms1280`.

[12]B. Ziberi, M. Cornejo, F. Frost, and B. Rauschenbach, "Highly ordered nanopatterns on Ge and Si surfaces by ion beam sputtering", Journal of Physics: Condensed Matter **21**, 224003 (2009).

[13]W. L. Chan and E. Chason, "Stress evolution and defect diffusion in Cu during low energy ion irradiation: Experiments and modeling", Journal of Vacuum Science and Technology A **26**, 1 (2008).

[14]M. Castro and R. Cuerno, "Hydrodynamic approach to surface pattern formation by ion beams", Applied Surface Science **258**, 4171–4178 (2012).

[15]Q. Wei, J. Lian, S. Zhu, W. Li, K. Sun, and L. Wang, "Ordered nanocrystals on argon ion sputtered polymer film", Chemical Physics Letters **452**, 124–128 (2008).

[16]S. A. Norris, J. C. Perkinson, M. Mokhtarzadeh, E. Anzenberg, M. J. Aziz, and K. F. Ludwig, Jr., "Distinguishing physical mechanisms using GISAXS experiments and linear theory: the importance of high wavenumbers", Scientific Reports, in press (2017).

[17]E. Anzenberg, C. S. Madi, M. J. Aziz, and K. F. Ludwig, Jr., "Time-resolved measurements of nanoscale surface pattern formation kinetics in two dimensions on ion-irradiated Si", Physical Review B **84**, 214108 (2011).

[18]E. Anzenberg, J. C. Perkinson, C. S. Madi, M. J. Aziz, and K. F. Ludwig, Jr., "Nanoscale surface pattern formation kinetics on germanium irradiated by Kr^+ ions", Physical Review B **86**, 245412 (2012).

[19]D. Adams, M. Vasile, T. Mayer, and V. Hodges, "Focused ion beam milling of diamond: Effects of H_2O on yield, surface morphology, and microstructure", Journal of Vacuum Science and Technology B: Microelectronics and Nanometer Structures Processing, Measurement, and Phenomena **21**, 2334–2343 (2003).

[20]R. Gago, L. Vázquez, R. Cuerno, M. Varela, C. Ballesteros, and J. Albella, "Nanopatterning of silicon surfaces by low-energy ion-beam sputtering: dependence on the angle of ion incidence", Nanotechnology **13**, 304–308 (2002).

[21]T. Chini, D. Datta, and S. Bhattacharyya, "Ripple formation on silicon by medium energy ion bombardment", Journal of Physics: Condensed Matter **21**, 224004 (2009).

[22]R. Cuerno and A.-L. Barabási, "Dynamic scaling of ion-sputtered surfaces", Physical Review Letters **74**, 4746–4749 (1995).

[23]H. H. Chen, O. A. Urquidez, S. Ichim, L. H. Rodriquez, M. P. Brenner, and M. J. Aziz, "Shocks in ion sputtering sharpen steep surface features", Science **310**, 294–297 (2005).

[24]M. Holmes-Cerfon, M. J. Aziz, and M. P. Brenner, "Creating sharp features by colliding shocks on uniformly irradiated surfaces", Physical Review B **85** (2012) `http://dx.doi.org/10.1103/PhysRevB.85.165441`.

[25]M. Holmes-Cerfon, W. Zhou, A. L. Bertozzi, M. P. Brenner, and M. J. Aziz, "Development of knife-edge ridges on ion-bombarded surfaces", Applied Physics Letters **101** (2012) `http://dx.doi.org/10.1063/1.4755838`.

[26]S. K. Sinha, E. B. Sirota, S. Garoff, and H. B. Stanley, "X-ray and neutron scattering from rough surfaces", Physical Review B **38**, 2297–2311 (1988).

[27]*DECTRIS*, `http://www.dectris.com`, Accessed: 2017 March 22.

[28]J. C. Perkinson, M. J. Aziz, M. P. Brenner, and M. Holmes-Cerfon, "Designing steep, sharp patterns on uniformly ion-bombarded surfaces", Proceedings of the National Academy of Arts and Sciences of the United States of America **113**, 11425–11430 (2016).

[29]I. Horcas, R. Fernandez, J. M. Gomez-Rodriguez, J. Colchero, J. Gomez-Herrero, and A. M. Baro, "WSXM: A software for scanning probe microscopy and a tool for nanotechnology", Review of Scientific Instruments **78**, 013705 (2007).

[30]S. Balay, S. Abhyankar, M. Adams, J. Brown, P. Brune, K. Buschelman, L. Dalcin, V. Eijkhout, W. Gropp, D. Kaushik, M. Knepley, D. May, L. C. McInnes, K. Rupp, B. Smith, S. Zampini, H. Zhang, and H. Zhang, *PETSc Web page*, `http://www.mcs.anl.gov/petsc`, 2017.

[31]S. Balay, S. Abhyankar, M. Adams, J. Brown, P. Brune, K. Buschelman, L. Dalcin, V. Eijkhout, W. Gropp, D. Kaushik, M. Knepley, D. May, L. C. McInnes, K. Rupp, P. Sanan, B. Smith, S. Zampini, H. Zhang, and H. Zhang, *PETSc users manual*, tech. rep. ANL-95/11 - Revision 3.8 (Argonne National Laboratory, 2017).

[32]S. Balay, W. D. Gropp, L. C. McInnes, and B. F. Smith, "Efficient management of parallelism in object oriented numerical software libraries", in Modern software tools in scientific computing, edited by E. Arge, A. M. Bruaset, and H. P. Langtangen (1997), pp. 163–202.

[33]M. Rauscher, T. Salditt, and H. Spohn, "Small-angle x-ray scattering under grazing incidence: The cross section in the distorted-wave Born approximation", Physical Review B **52**, 16855–16863 (1995).

[34]E. Gullikson, *X-Ray Interactions With Matter. The Center For X-Ray Optics*, July 2016.

[35]B. L. Henke, E. M. Gullikson, and J. C. Davis, "X-ray interactions: photoabsorption, scattering, transmission, and reflection at E=50-30000 eV, Z=1-92", Atomic Data and Nuclear Data Tables **54**, 181–342 (1993).

[36]Y.Ishii, C. S. Madi, M. J. Aziz, and E. Chason, "Stress evolution in Si during low-energy ion bombardment", Journal of Materials Research **29**, 2942–2948 (2014).

[37]Y. Yoneda, "Anomalous surface reflection of x rays", Physical Review **131**, 2010–2013 (1963).

[38]M. Cross and P. Hohenberg, "Pattern formation outside of equilibrium", Reviews of Modern Physics **65**, 851–1112 (1993).

[39]"Pattern Formation and Dynamics in Nonequilibrium Systems", in, edited by M. Cross and H. Greenside (Cambridge University Press, 2009).